IEEE Access
Multidisciplinary | Rapid Review | Open Access Journal

Received March 27, 2017, accepted April 25, 2017, date of publication May 9, 2017, date of current version June 7, 2017.

Digital Object Identifier 10.1109/ACCESS.2017.2702643

A Comparison of Techniques for Fault Detection in Inverter-Fed Induction Motors in Transient Regime

VANESSA FERNANDEZ-CAVERO[1], DANIEL MORINIGO-SOTELO[1,2], (Member, IEEE), OSCAR DUQUE-PEREZ[1], AND JOAN PONS-LLINARES[3], (Member, IEEE)

[1]University of Valladolid, 47011 Valladolid, Spain
[2]HSPdigital Research Group, Salamanca, Guanajuato 36730, México
[3]Instituto de Ingeniería Energética, Universitat Politècnica de València, 46022 València, Spain

Corresponding author: Daniel Morinigo-Sotelo (daniel.morinigo@eii.uva.es)

This work was supported in part by the Spanish Ministerio de Economía y Competitividad and in part by the FEDER program in the framework of the Proyectos I+D del Subprograma de Generación de Conocimiento, Programa Estatal de Fomento de la Investigación Científica y Técnica de Excelencia under Grant DPI2014-52842-P.

ABSTRACT Fault detection in induction motors operating in non-stationary regimes has become a need in today's industry. Most of the works published deal with line-fed motors. Nevertheless, the number of inverter-fed induction motors has significantly increased in recent years. Therefore, several fault detection techniques have been proposed lately for this type of motors, based mainly on an adequate input signal processing to obtain fault signatures in the time-frequency domain. In this paper, a comparison of time-frequency techniques applied to fault detection in inverter-fed induction motors in a transient state is presented. For that purpose, the techniques are applied to two current signals acquired from two induction motors with two types of faults: bar breakage and mixed eccentricity. The paper shows the particularities and special difficulties of diagnosing under this type of feeding, reviewing the works related to each technique. The strengths and weaknesses of these techniques are discussed with the goal of providing a criterion for its application in an industrial environment and guidance for future developments in this field.

INDEX TERMS Time-frequency decomposition, induction motors, inverters, fault detection, transient regime.

I. INTRODUCTION

Fixed speed operation of induction motors (IM) has a significant impact on its power consumption and operational costs over its lifetime. Therefore, these uses are considered as very inefficient. If the motor is inverter-fed, the speed can be regulated and adapted to the actual requirements of the load, which results in important energy savings [1]. For example, a motor running at half speed reduces its consumption by 75% [2]. Recent European Union directives encourage the use of energy-efficient motors, or the use of regular ones along with inverters and this explains why the number of inverter-fed induction motors has significantly increased. There are other applications where IMs usually do not operate at steady-state, and the use of an inverter is mandatory as in electric traction [3] or in manufacturing processes where flexibility is a need [4].

This change in the electric drives field also has a substantial impact on maintenance. A predictive maintenance procedure tries to detect a fault in advance and to assess its severity to begin the fixing process, minimizing the economic implications of a future failure [5]. In the case of IM, these procedures rely mainly on the monitoring and analysis of the stator current and mechanical vibrations [6]–[9]. The first method, known as Motor Current Signature Analysis (MCSA), is non-invasive, which constitutes its primary benefit over other monitoring schemes. However, since it is based on the use of the Fast Fourier Transform (FFT), it is not appropriate for applications where the motor speed is subject to continuous changes [10]. Even if there are long enough periods of steady state operation, in inverter-fed IM, the current spectrum is rich in harmonic content originated by the switching mechanism of the inverter and usually, the signal has a high noise level. Some harmonics originated by the supply can overlap with fault-related harmonics, making their observation and subsequent diagnosis more complicated. Additionally, the amplitude of some fault related harmonics also depends on the

output assigned frequency or the inverter control type [11]–[13]. All this has originated an active field of research on fault detection and diagnosis in inverter-fed IM and in transient regimes.

In IM transient regimes, other mathematical transformations than the FFT are needed and are being developed to analyze the stator current. These mathematical tools belong to the field of Time-Frequency Decomposition (TFD) tools. It is reported in the literature the use of techniques such as wavelet-based transforms or the Wigner-Ville Distribution (WVD) to detect faults in direct-line fed IM during the startup [14], [15]. Their application to inverter-fed IM is not straightforward. The principal difference between direct-line and inverter-fed IM startups is that the slip frequency is low during the whole transient (besides, the fundamental frequency changes). Consequently, the trajectories of some fault related harmonics are very close to the trajectory of the main frequency component. As it will be explained in Section II, this is the essential characteristic that makes fault detection in inverter-fed IM so different compared to direct-line IM. In these circumstances, the detectability of the fault will rely on the time and frequency resolution capabilities of the mathematical transformation used to process the stator current signal.

This paper, which takes as its starting point the conference paper [16], provides valuable knowledge on this topic: the main techniques present in the technical literature are reviewed and their performance for fault detection in the time-frequency plane is compared. For this purpose, two startup currents corresponding to two faulty inverter-fed IM (bar breakage and eccentricity faults) are analyzed with each considered transform. The paper shows which techniques are capable of generating a time-frequency graph in which the fault related harmonics are distinguished from the high energy main component (comparison of fault quantification techniques would be the next step, being out of the paper scope). More precisely, the paper exposes the advantages and drawbacks of each technique in terms of time and frequency resolution. Moreover, it exhibits the weak points not yet resolved, opening new paths of research.

II. FAULT HARMONIC TRAJECTORIES IN THE TIME-FREQUENCY PLANE

In transient regimes, fault detection techniques rely on the ability to track low-energy fault related harmonics in comparison to the high-energy Fundamental Component (FC, first harmonic of the signal) and other harmonics such as the winding and principal slot harmonics. In this paper, the study is focused on the detection of broken rotor bars and mixed eccentricity in transient regimes. In the MCSA field, these faults are identified by the presence of specific components in the stator current spectrum, whose frequencies are already known [17], [18]. These faults mainly manifest themselves by a pair of bands around the FC, whose characteristic frequency depends on the motor load through the slip as follows:

- Broken Rotor Bar (BRB) frequencies:
  - Lower Sideband Harmonic (LSH):

$$f_{LSH} = (1 - 2s) f_s \tag{1}$$

  - Upper Sideband Harmonic (USH):

$$f_{USH} = (1 + 2s) f_s \tag{2}$$

- Mixed Eccentricity Related-Harmonics (ERH):
  - Lower Sideband Harmonic (ERHn):

$$f_{ERHn} = \left(1 - \left(\frac{1 - s}{p}\right)\right) f_s \tag{3}$$

  - Upper Sideband Harmonic (ERHp):

$$f_{ERHp} = \left(1 + \left(\frac{1 - s}{p}\right)\right) f_s \tag{4}$$

where s is the slip, p is the number of motor pole pairs, and f_s is the main frequency of the supply voltage. If the time evolutions of s and f_s are obtained, these expressions are also used in transient regimes. The slip is given by:

$$s = \frac{n_1 - n}{n_1} \tag{5}$$

where n_1 is the synchronous speed, given by: $n_1 = 60 f_s / p$ and n is the rotor speed.

In line-fed IM, the FC frequency is fixed and established from the very first moment of the motor startup. Therefore, the synchronous speed is also constant. As the rotor speed, in a standard startup, increases almost linearly from zero to nearly the synchronous speed, the slip decreases from 1 almost linearly to a very low value. Due to these evolutions, the trajectory of some fault harmonics is very advantageous for monitoring purposes because they evolve far from the FC, at least during the startup. For example, the LSH traces a trajectory with a characteristic V-pattern [19] during a line-fed IM startup, as it is shown in Fig. 1(a) (assuming a linear evolution of the slip vs. time). The trajectories of the USH, ERHn, and ERHp are also observed for a motor with two pairs of poles. In inverter-fed IM, the harmonics time-evolution during the startup is very different from the line-fed case [3], [10] as it can be observed comparing Figs. 1(a) and (b). An inverter permits to avoid the typical inrush current of line-fed IM startups and to control the duration of this transient. As a result, the startup is smooth and free of high torques. Regardless of the type of IM control, the FC of the inverter output voltage is increased from 0 Hz to the final operating frequency. Furthermore, as the motor speed increases parallel to the synchronous speed and very close to it, the slip frequency sf_s is very low. Accordingly, the LSH and USH (which have low energy) evolve during the startup parallel and close to the FC (highest energy harmonic), making their detection especially difficult due to the difference in energies between them. Conversely, the time evolution of ERHn and ERHp is more advantageous for detection purposes.

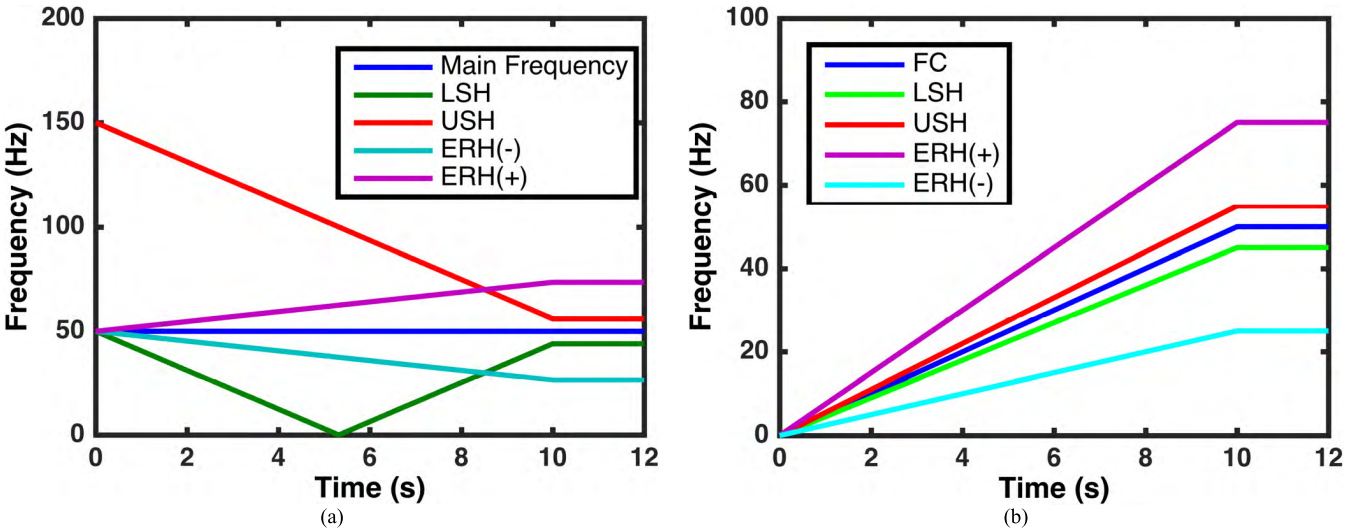

FIGURE 1. Theoretical trajectories of fault related harmonics: (a) 10 s long line-fed IM startup (supposing a linear evolution of the slip vs. time); (b) 10 s long inverter-fed IM startup with a linear evolution of the main frequency from 0 to 50 Hz.

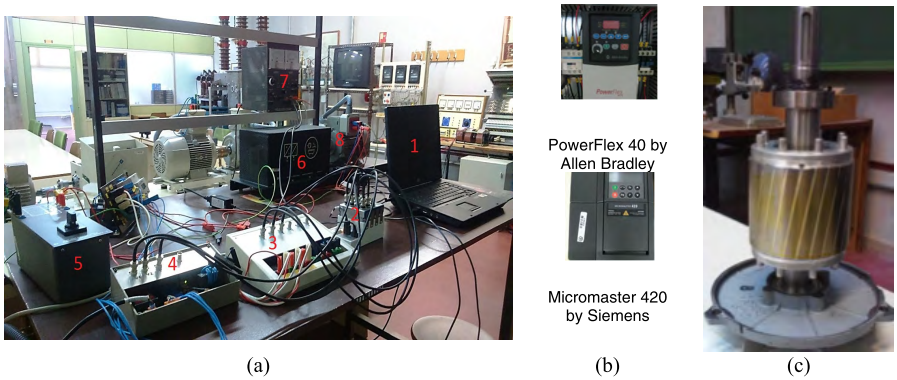

FIGURE 2. (a) Laboratory test bench; 1) PC; 2) DAQ board; 3) and 4) custom-made sensors boards; 5) switch; 6) electromagnetic brake; 7) brake control unit; 8) induction motor; (b) Inverters; (c) IM rotor cage with a drilled hole to simulate a broken bar.

III. CASES OF STUDY

Two Siemens IM are tested on a laboratory test bench (Fig. 2(a)) at different conditions and fed by two inverters (Fig. 2(b)). Both IM have the following characteristics: rated power of 1.1 kW, star connection, 400 V rated voltage, 1410 rpm rated speed and 2.6 A rated current. The motor load is a powder electromagnetic brake by Lucas Nülle. The acquisition system is based on a PC with an NI cDAQ-9174 USB acquisition board. A Hall effect sensor by LEM is used as a current transducer.

The first IM has a broken rotor bar caused by drilling a hole in the rotor cage (Fig. 2(c)) and is fed with an Allen Bradley PowerFlex 40 inverter. This inverter is programmed to provide a 10 s startup with the output frequency increasing linearly from 0 to 50 Hz. The stator current (Signal 1) is captured at 5 kHz as sampling frequency (Fig. 3(a)), including the startup and a long steady state where the motor consumes 2.4 A. The trajectory of the FC in the time-frequency (t-f) plane is shown in Fig. 3(b).

The second IM has a high level of mixed eccentricity caused by a misalignment between the motor and the brake. This motor is fed by a Siemens Micromaster 420 inverter. The startup is programmed to last 2.2 s with the output frequency increasing linearly from 0 to 50 Hz. The stator current (Signal 2), captured at 1 kHz (Fig. 4(a)), also includes the startup followed by a steady state where the motor consumes 2.55 A. The trajectory of its FC in the t-f plane is shown in Fig. 4(b).

The slips of the two IM at the final steady state, calculated through the speed and the FC frequency, are 0.042 and 0.045. Therefore, the fault frequencies at this steady operation and according to equations (1) to (4) are:

- Signal 1 (Fig. 5(a), IM with BRB): LSH and USH, 45.8 Hz and 54.2 Hz.
- Signal 2 (Fig. 5(b), IM with mixed eccentricity): ERHn and ERHp, 27.9 Hz and 72.2 Hz.

These fault related harmonics have high amplitudes in its respective power spectral densities (PSD), which confirm that

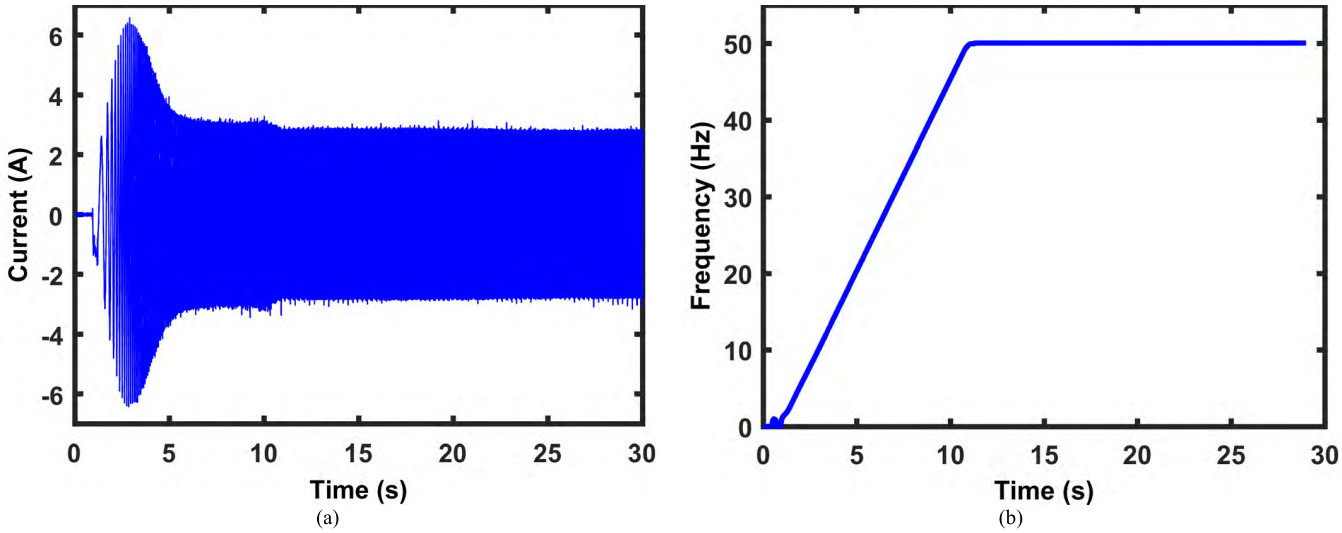

FIGURE 3. Signal 1: (a) Stator current of the IM with a broken rotor bar; (b) Trajectory of the first harmonic in the t-f plane.

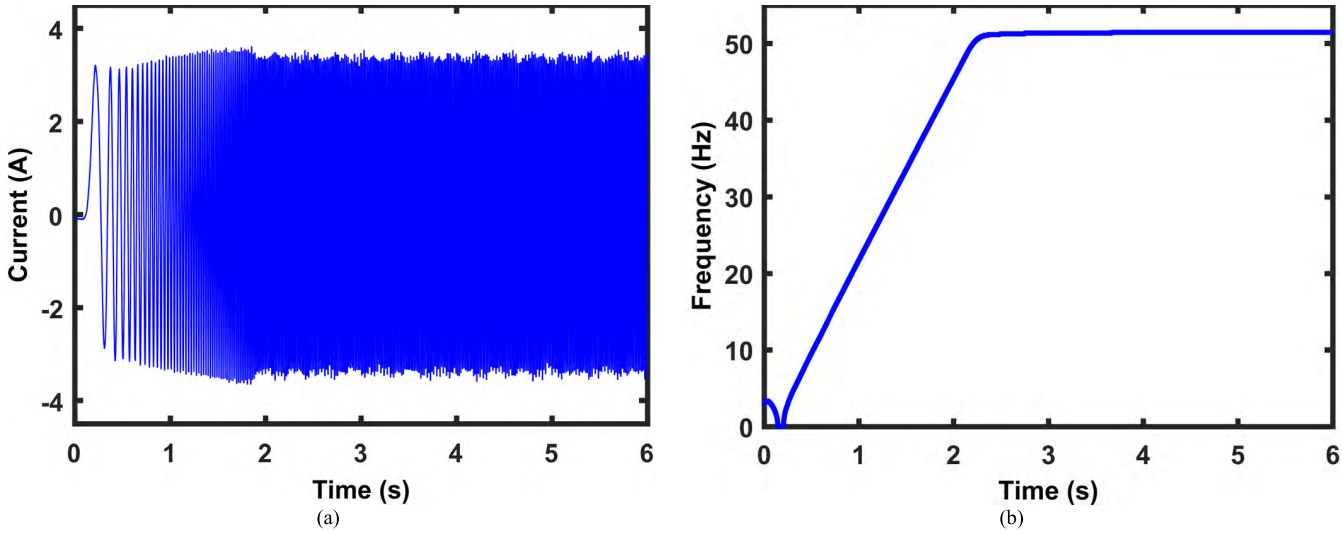

FIGURE 4. Signal 2: (a) Stator current of the IM with a high mixed eccentricity; (b) Trajectory of the first harmonic in the t-f plane.

these motors are suffering the previously mentioned faults. Figs. 5(a) and (b) show the PSD of the stator current of the two IM.

IV. FAULT DETECTION TECHNIQUES BASED ON TIME-FREQUENCY ANALYSIS IN INVERTED-FED INDUCTION MOTORS

In this Section, the most significant tools used for fault detection in inverter-fed IM in transient regimes are analyzed and compared through its application to two experimentally acquired signals (Section III). Testing the techniques with the same two currents enables to clarify their advantages and drawbacks, and show which are useful and which are not, what is a significant contribution for field engineers who need to choose the best tool to perform a diagnosis. Moreover, unsolved problems are pointed out, showing possible trends in research.

For each technique, its characteristics are described, showing its inherent advantages and drawbacks, briefly referencing works where it has been used with directly-fed IM, and reviewing the works dealing with inverter-fed IM. Then, a deep analysis of the results when analyzing the two currents in Section III is presented, explaining them according to the technique characteristics previously described. Before this, Subsection A presents the results of applying the FFT, showing what can be seen in its spectrum, and what we will try to obtain with a t-f transform.

A. FAST FOURIER TRANSFORM

FFT is the base of the analysis of the stator current of IM in steady-state regimes. It provides information about the

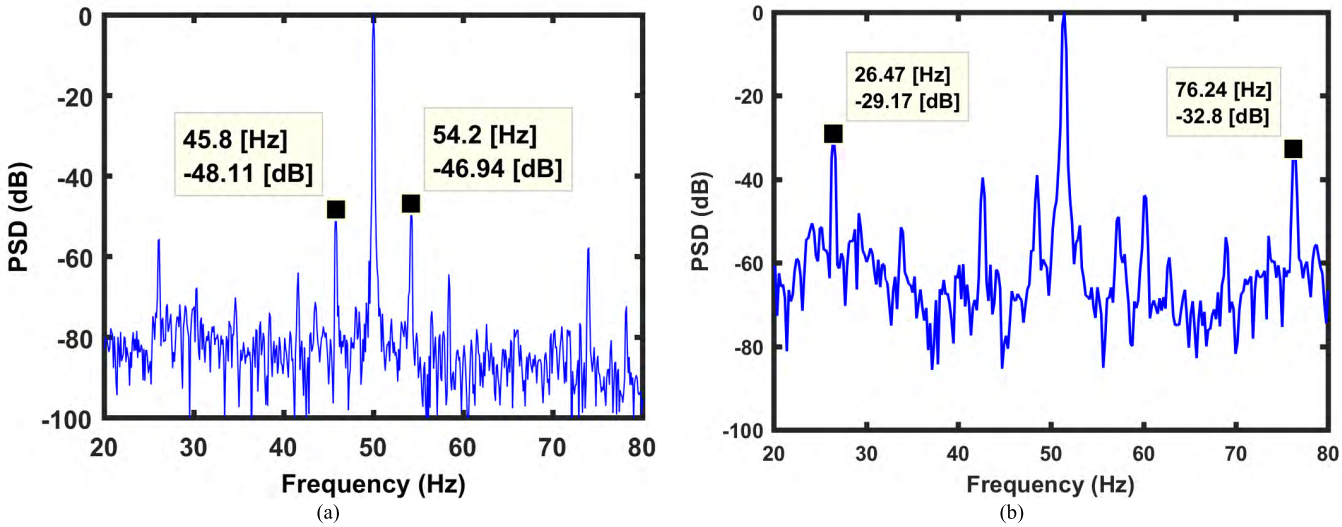

FIGURE 5. PSD of: (a) the IM with a BRB and fed by the Allen Bradley inverter; (b) the IM with mixed eccentricity fed by the Siemens inverter.

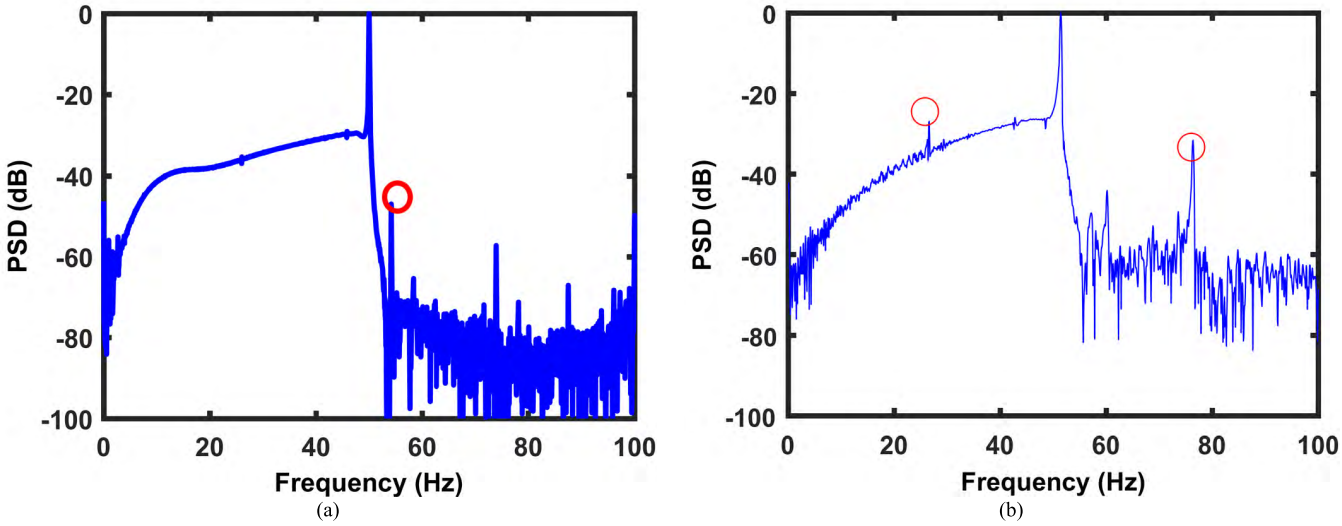

FIGURE 6. PSD of Signal 1 (a) and Signal 2 (b).

harmonic content of a periodic signal and the energy associated to each harmonic. Fault detection is carried out by identifying certain frequencies in the stator current spectrum. If the current is non-periodic (IM in transient regime), FFT is not suitable for fault detection: in those cases, it is important to know the signal harmonic content and the time evolution of these harmonics (unfortunately, this information is not provided by the FFT).

The two proposed signals have been analyzed with the FFT. Figs. 6(a) and (b) show the spectra, which are consistent with the technique capabilities and the harmonic content of the two transient signals. Both spectra display an almost continuous harmonic content from 0 to 50 Hz, explained by the linear increment of the FC of the inverter output voltage during the startup, which evolves from 0 to 50 Hz. The energy of this harmonic is much higher than the energy of the rest of harmonics and dominates the spectrum in that frequency range. Consequently, it is impossible to observe any other components, such as the fault related harmonics. The only exception is the presence of a small peak above the FC energy at 26.34 Hz in Fig. 6(b), related to the ERHn at steady state.

The FC frequency at steady state is perfectly identified (50Hz) as well as other harmonics above. The USH is observed in Fig. 6(a) and the ERHp in Fig. 6(b) as well. These harmonics are observed due to the long steady state captured.

These results demonstrate that this technique is not suitable for fault detection in transient states because it does not provide information about the time development of the harmonics and it is not possible to identify their characteristic trajectories.

A Fourier-Bessel expansion is proposed in [20] to overcome the limitation of the FFT with non-stationary signals. Another approach to overcome the FFT limitations is presented in [21] where the Fractional FFT is proposed to detect broken bars. Nevertheless, both references deal with directly-fed IM.

B. SHORT TIME FOURIER TRANSFORM

The Short-Time Fourier Transform (STFT) is considered as the standard transform in the t-f domain, and the rest of transforms are usually compared to it [22]. As nearly all linear transforms (transforms in subsections C and F, but not transform in subsection G), the STFT is based on the use of a time window whose length fixes the time and frequency resolutions, which are not independent. A long window length means a good frequency resolution, but time resolution is decreased. A short window length improves time resolution at the cost of worsening frequency resolution. In the case of the STFT, this tradeoff is the same for every point in the t-f plane analyzed: once fixed in a point, it cannot be changed at different points. This is the main limitation of this technique. Due to its limitations regarding resolution, few works report its use. In [24], the STFT is used to detect faults in directly-fed IM. No paper deals with inverter-fed IM.

To calculate the STFT, the time window is centered in the time instant and modulated at the frequency where the transform needs to be calculated. Then, the modulated window is correlated with the signal to be analyzed. The modulated window is called a t-f atom: a function whose energy is concentrated at a point of the t-f plane (the instant where the window is centered and the frequency at which is modulated). The result of the correlation is a measure of the energy density of the analyzed signal, around the point of the atom's center. If this operation is repeated in a big set of points of the t-f plane, by centering the atom each time in a different t-f point until creating a big grid, the energy density of the analyzed signal along the plane is obtained. All linear transforms (subsections C, F and G) follow this same mathematical structure: the correlation of a signal with a family of time-frequency atoms. In this paper, for the sake of a fair comparison, all the atoms are based on frequency B-spline functions [27].

The result of a t-f transform is a two-dimensional representation of the signal in the t-f plane (its t-f energy distribution), showing the trajectories of the frequency components. The spectrograms resulting from analyzing the two signals presented in Section III with the STFT are shown in Figs. 7(a) and (c). The ideal result would be to obtain the evolution of a signal component in the t-f plane as a perfectly thin line. Nevertheless, in this type of linear transforms (STFT, wavelets, etc.), the evolution appears as a line with a certain thickness, and this is due to the tradeoff mentioned earlier, related to the use of t-f atoms, as further explained below.

The families of atoms that have been used to generate the resulting STFT spectrograms are presented in Figs. 7(b) and (d). More precisely, these figures show the energy distribution of some of the t-f atoms used. As explained before, the atom captures the energy of the signal in the zone of the t-f plane where the atom's energy is concentrated. In other words, the atom acts like a t-f filter, capturing the signal's energy in a small region around the analyzed point. If the atom is long in time, when centering it in a point and correlating with the signal, it is obtained information related to many time instants. Therefore, the time resolution is bad. The drawback appears when, trying to shorten the atom in time, inevitably the atom lengthens in frequency and when correlating it with the signal, associated to the atom's frequency center, it is obtained information of the signal related to many frequencies. Therefore, the frequency resolution is poor. That is, the atom cannot filter well in time and frequency simultaneously because if its energy is concentrated in time, it spreads in frequency, and vice versa. Moreover, in the case of the STFT, the type of atom is the same at every point of the plane analyzed, as it can be seen in Figs. 7(b) and (d). Therefore, the typical tradeoff of linear transforms between time and frequency resolutions is, in the case of the STFT, the same for every point analyzed.

If an atom is centered at a point of the FC evolution, the longer the atom is in time, the more it has to be shifted in time to stop capturing energy from that FC. Therefore, a long atom in time increases the thickness in time with which the evolution of the FC is captured. On the other hand, the longer the atom is in frequency, the more it is needed to separate it from the FC along the frequency axis to stop capturing its energy, and the thicker would be the representation of the FC in the STFT result. The FC evolution shown in the spectrogram will have a thickness in time and frequency (measured along the time and frequency axes respectively), which depends on how much the energy of the atom spreads along time and along frequency. Since the atom cannot be shortened in time and in frequency simultaneously, the thickness of the evolution obtained cannot be diminished both along the time and frequency axes. Therefore, the line representing the time-frequency evolution always will have a certain minimum thickness.

For a horizontal evolution, an atom long in time and short in frequency must be used: the thickness along the frequency axis would be low and the frequency of the component would be established with precision (good frequency resolution). For a vertical evolution, the atom needs to be long in frequency and short in time: the thickness along the time axis would be low and the instant where the frequency changes abruptly would be well determined (good time resolution). If the frequency-time evolution is arbitrary, the slope criterion [23] establishes that the proportion between the atom's length along the frequency axis and the atom's length along the time axis must be equal to the proportion between how much the component's frequency changes and the time interval it takes to perform that change, i.e., equal to the time derivative of the component's frequency to be captured. The slope criterion enables to choose the atom which ensures a tradeoff between time and frequency resolution, such as the

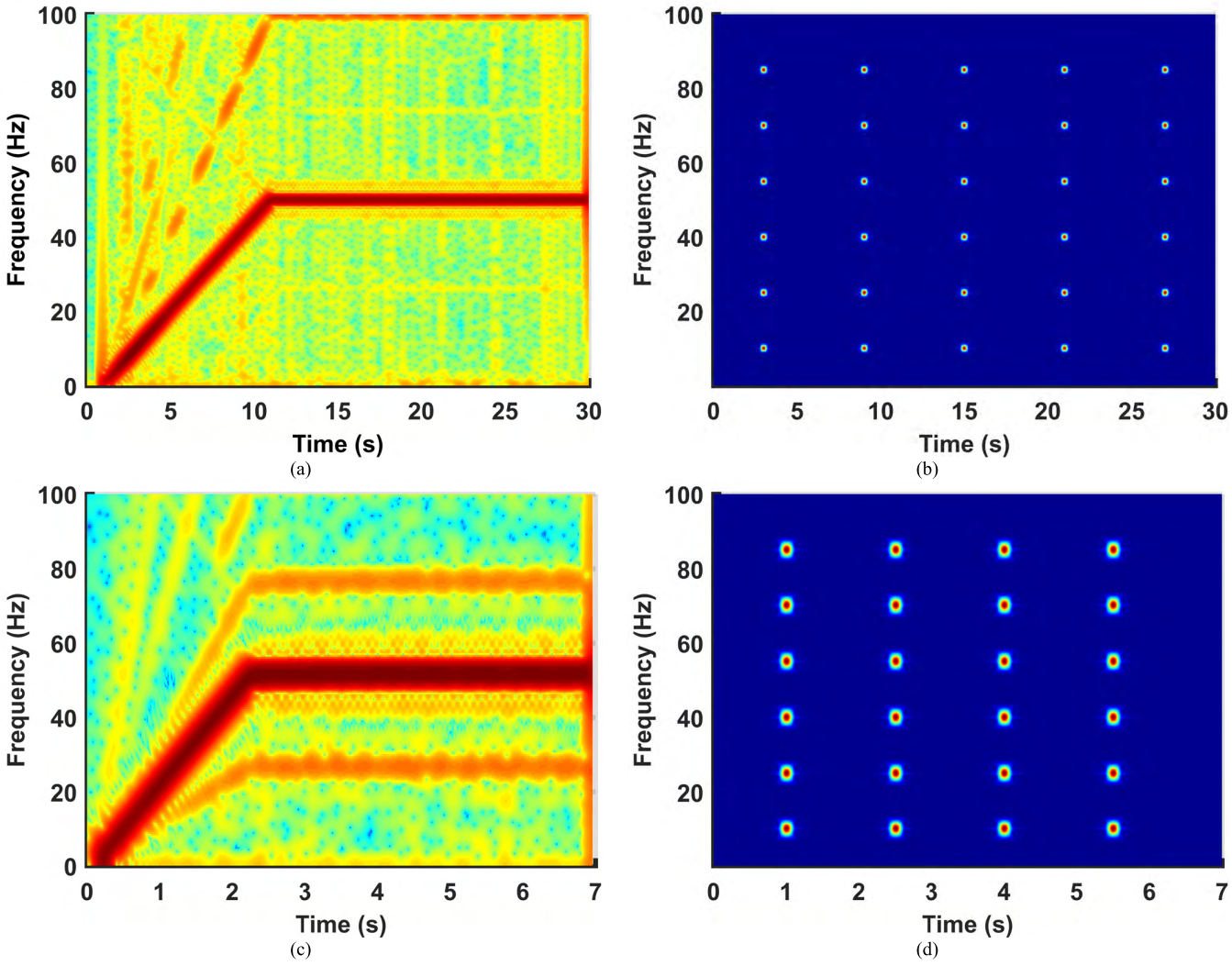

FIGURE 7. STFT spectrograms and atoms for Signal 1 ((a) and (b)) and for Signal 2 ((c) and (d)).

width of the line (measured perpendicularly to the component evolution) reaches a minimum.

For the two signals analyzed through the paper, the slope criterion is applied [23] fixing this tradeoff (adjusting the window length) to optimize the capture of the FC evolution during the startup. This way, the family of atoms to be used is established (Figs. 7(b) and (d)). As a consequence, the global thickness of the FC during the startup is minimized, tending as much as possible to the ideal result: a perfectly thin line.

In the case of a bar breakage (Signal 1), this FC minimum thickness is not sufficient to observe the trajectories of the BRB harmonics during the IM startup. As it is seen in Fig. 1(b), the BRB harmonics evolve very closely to the FC. Therefore, their evolutions are always inside the thickness of the line showing the FC trajectory (Fig. 7(a)), which has been minimized with the slope criterion. On the other hand, the frequency resolution obtained is high enough to distinguish the BRB related harmonics during the final steady state: the FC thickness in the frequency axis direction is sufficiently small to separate the BRB harmonics from the FC. Concerning Signal 2, the mixed eccentricity harmonics evolve far enough from the FC (Fig. 1(b)). Therefore, their trajectories can be observed during nearly the whole capture (Fig. 7(c)), except for the first half of the startup (below 1 second), when they are yet too close to the FC.

Additional trajectories around the FC are observed in the steady-state regime in the case of Signal 2 (Fig. 7(c)). These harmonics are produced by the switching mechanism of the inverter, but the resolution limitations of the STFT do not permit to observe them correctly, and they can be confused with BRB harmonics.

Concluding, this technique facilitates the observation of certain low-energy harmonics that are distant from the high-energy FC, as it happens with the mixed-eccentricity fault. However, if these harmonics are very close to the FC, as it occurs in the case of BRB fault, the best achievable resolution in the t-f plane is not sufficient to distinguish them.

C. WAVELETS

The Continuous Wavelet Transform (CWT) is similar to the STFT: the signal to analyze is correlated with a function called wavelet (which is a t-f atom with specific characteristics). Nevertheless, while the STFT uses a fixed length windowing function (fixed t-f resolution tradeoff along the plane), the wavelet time length depends on the frequency analyzed [25]. As a result, this transform provides a poor frequency resolution and a better time resolution at high frequencies. On the other hand, at low frequencies, the frequency resolution is much better and the time resolution worsens. The Discrete Wavelet Transform (DWT) is the discrete version of the CWT, which is commonly used to obtain the energy distribution of a signal in the t-f plane. The DWT is used to perform a decomposition of the signal into a previously selected number of frequency bands, whose bandwidths follow a dyadic scale fixed by the signal sampling frequency and the number of decomposition levels chosen [26].

The use of the CWT to detect faults in IM is reported in the literature. Nevertheless, the works published are mainly centered in directly-fed motors [27], [28], and very few papers deal with inverted-fed IM in transient regime. For instance, the CWT is used in [29] to detect mixed eccentricity in an inverter-fed IM, obtaining a t-f plot of the stator current. The t-f resolution achieved permits to track the evolution of the mixed eccentricity-related harmonics during transients such as a startup where the main frequency increases linearly from 0 to 50 Hz, or other changes in the inverter output assigned frequency. Nevertheless, as explained below, this type of transform is less suited than the STFT to detect the fault harmonics evolutions.

The use of the DWT has been widely reported in the literature. As with the CWT, the works are predominantly related to directly-fed IM, detecting faults generally through transient currents [30], and recently using other signals as the reactive [31] and apparent power [32]. Research work trying to detect faults in inverter-fed IM has also been published. In [33], a variant of DWT, known as Wavelet Packets Decomposition (WPD), is used for early detection of bearing faults in inverter-fed IM. Nonetheless, only the DWT subsignal that contains fault component is used; the DWT acts only as a filter and its capabilities as a t-f transform are not explored. Finally, another application of the DWT is presented in [34], where it is used along with the WPD to detect stator inter-turn faults during the startup of an inverter-fed IM. The evolution of the faulty component is identified only at the last second of an 8.5 s startup.

The two proposed signals have been analyzed using the CWT. The results, shown in Figs. 8(a) and (c), illustrate the characteristics of this transform. The wavelet/atom features have been chosen to optimize the capture of the FC at the point where its frequency reaches 25 Hz, according to the slope criterion [23], as with the STFT. Therefore, the tradeoff between time and frequency resolution is the same as with the STFT at that frequency, and this enables to minimize, at that point, the thickness of the line which represents the FC evolution. However, what happens at higher and lower frequencies?

Figs. 8(b) and (d) show the families of atoms used to generate the CWT spectrograms of signals 1 and 2 respectively. Comparing with the atoms used to produce the STFT spectrograms (Figs. 7(b) and (d)), only the atoms at 25 Hz are the same, while at the rest of frequencies are different. At low frequencies, these atoms display a large base (long in time, short in frequency). As the frequency increases, the shape of these atoms changes by an increment of their height and a decrease of their base (short in time, long in frequency). This explains why the time and frequency resolutions are not uniform in the whole t-f plane. The CWT spectrograms have a worse time resolution at low frequencies and a better frequency resolution at higher frequencies.

Summarizing, the CWT frequency resolution increases while the time resolution gets poorer at frequencies lower than 25 Hz. That is why the energy of the FC spreads over a wider time length than in the STFT result, hindering the observation of the fault related harmonics. At frequencies higher than 25 Hz, the time resolution increases, while the frequency resolution decreases. Nevertheless, the rate of change is not fast enough to clearly see the effect up to the highest frequency analyzed (it could be better observed at 1000 Hz instead of 100 Hz). In any case, this change in the tradeoff does not improve the capture of these evolutions as it is mainly suited to capture parabolic t-f evolutions. In fact, for both signals, at frequencies higher than 25 Hz, horizontal trajectories related to the steady state are found. As explained in the previous subsection, for those frequencies it would be desirable to have atoms long in time (the opposite to the CWT atoms), which increase the frequency resolution, and enable to determine the frequencies at this steady state operation better.

As a result, comparing Figs. 7(a) and 8(a), it can be seen that the bar breakage components are not detected during the startup in either of them. Moreover, comparing Figs. 7(c) and 8(c), the mixed eccentricity-related harmonics evolutions are exposed during a shorter time by the CWT. Concluding, the CWT does not improve the STFT results, and it should be avoided for the analysis of this type of signals. Finally, both signals are also decomposed with the DWT, but the distinctive evolutions of the faulty harmonics considered are not observed because in all obtained subsignals, in which the faulty harmonics are present, the FC is present too and, since it is very dominant, it masks the rest of harmonics.

D. WIGNER-VILLE DISTRIBUTION

When using the DWT and CWT, the time and frequency resolution cannot be improved simultaneously. The STFT has a fixed t-f resolution tradeoff while, in the case of the CWT, it varies with the analyzed frequency. The WVD, which belongs to the family of quadratic t-f representations, was defined to obtain a distribution of energy in the t-f plane without loss of resolution (i.e., highest resolution in both time

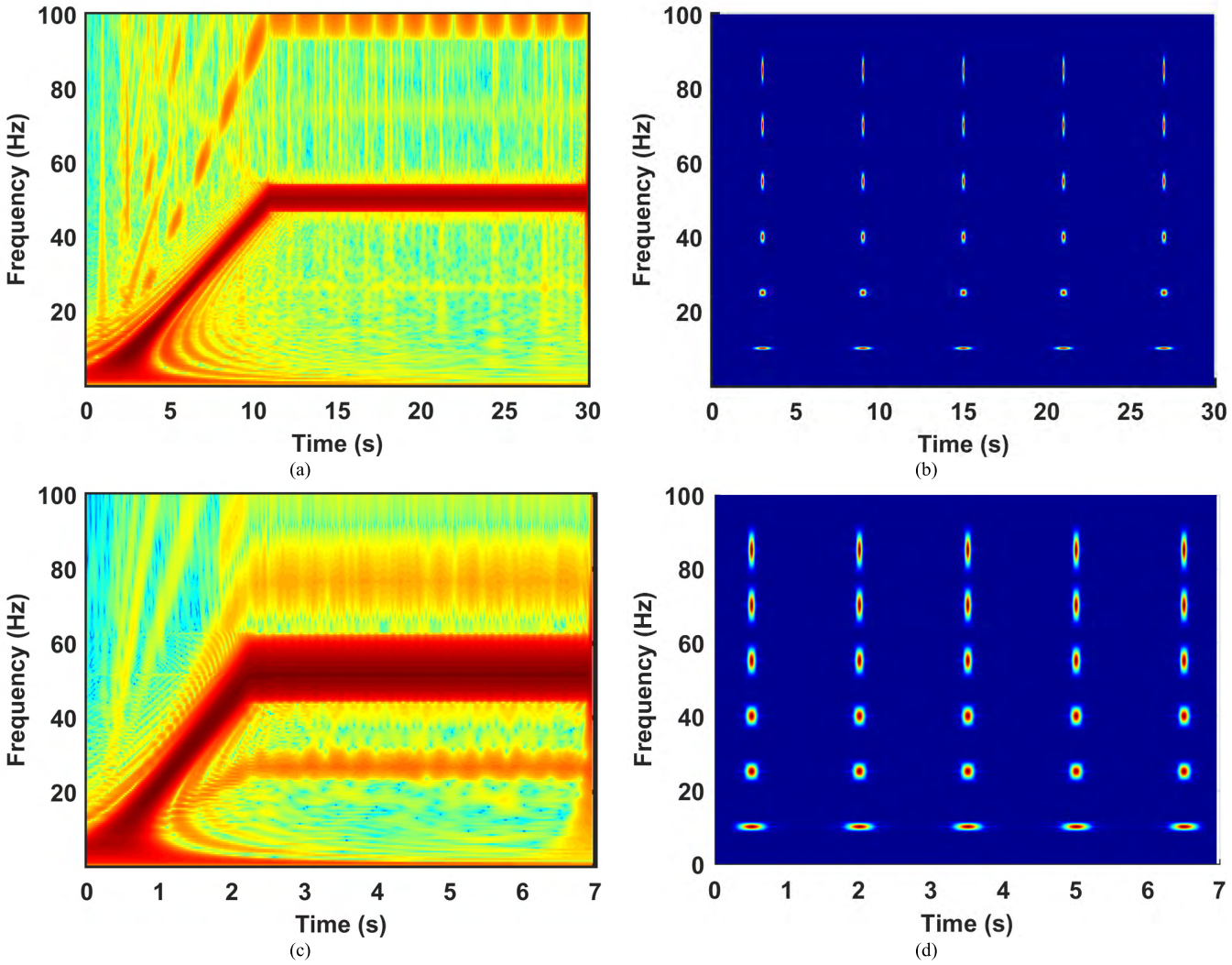

FIGURE 8. CWT spectrograms and atoms for Signal 1 ((a) and (b)) and for Signal 2 ((c) and (d)).

and frequency directions). In other words, while the STFT and CWT show the harmonics evolutions in the t-f plane as lines with a certain thickness, the WVD represents them as perfectly thin lines.

The major drawback of this transform is the presence of cross-term interferences in the t-f energy distribution when multicomponent signals are analyzed [35]. More precisely, for each pair of components in the signal, the WVD introduces a spurious component in the result called cross-term. When detecting rotor asymmetries and eccentricity in directly-fed IM, this effect has been reduced by filtering the FC and the winding harmonics (multiples of the FC) previously to the computation of the energy distribution [36]–[38]. Other authors have proposed the use of a modified WVD, in which a kernel smooths the WVD result reducing the cross-terms (mainly used for the detection of rotor faults in DC motors [39]). Nonetheless, the kernels introduce a t-f resolution tradeoff in the result, as with the STFT and CWT.

Up to date, there are no papers in the field applying the WVD to detect faults in inverter-fed IM. The principal drawback, in this case, is that the trajectories of the FC and its harmonics are no longer constant, as in the directly-fed case. Therefore, the approaches used before, based on filtering, cannot be applied to this type of signals. Moreover, the kernels cannot be as easily used as in the case of constant FC. Figs. 9(a) and (b), showing the WVD of the analyzed signals, are a clear demonstration of the main disadvantage of this technique. These signals contain many frequency components, and this is reflected in the WVD as a complex set of cross-terms, especially around the FC. The presence of cross-terms prevents the observation of the trajectories of the fault related harmonics or introduces new fake components that complicate a correct interpretation of the energy distributions. As a result, the bar breakage harmonics are not observed in Fig. 9(a), while only some traces of the mixed eccentricity harmonics are observed in Fig. 9(b).

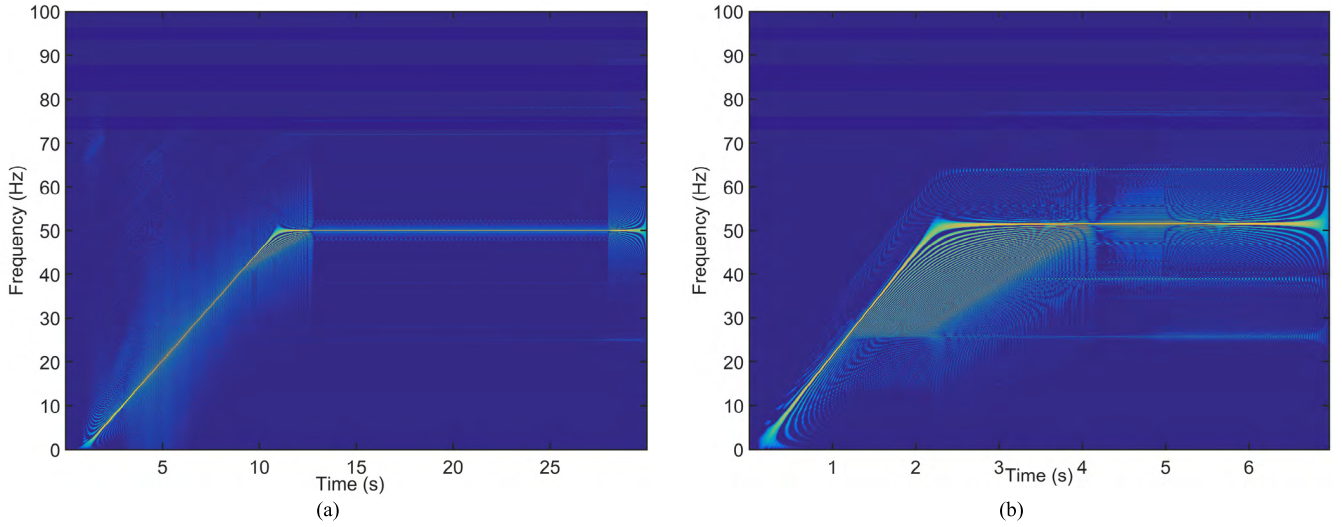

FIGURE 9. WVD spectrogram of Signal 1 (a) and Signal 2 (b).

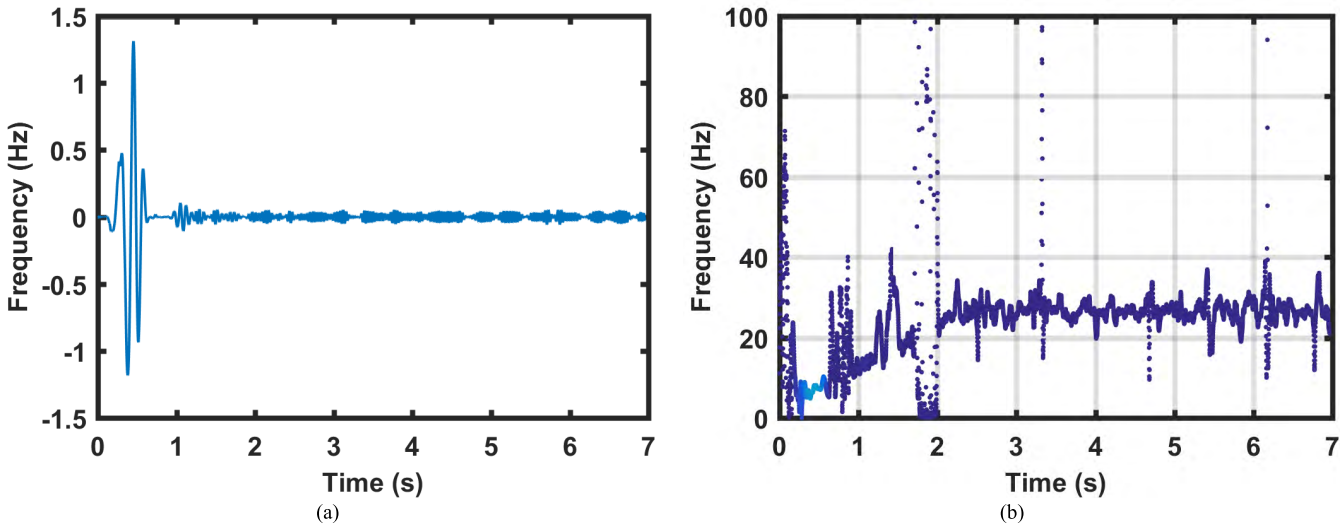

FIGURE 10. (a) IMF number 4, result of the CEEMD decomposition of Signal 2; (b) HHS of the IMF number 4 of Signal 2, showing the ERHn t-f evolution, related to the mixed-eccentricity fault.

E. HILBERT-HUANG TRANSFORM

The Hilbert-Huang Transform (HHT) is an empirical technique, combination of the Hilbert Spectral Analysis or Hilbert Transform (HT) and the Empirical Mode Decomposition (EMD). The HHT can deal with non-stationary and nonlinear signals. The EMD performs an adaptive decomposition, based on local characteristics of the signal, into a finite number of intrinsic mode functions (IMF). These IMF are individual signals, nearly monocomponent, more adequate for the use of the HT. The HT applied to the IMF leads to an identification of instantaneous frequencies and amplitudes with a physical meaning. The HT analysis of the original multicomponent and noisy signal generates spurious amplitudes without physical meaning. The EMD algorithm presents some drawbacks as border effects, mode mixing or uncertain stopping criterion. Some noised assisted methods have been developed to overcome these problems, as the Complete Ensemble Empirical Mode Decomposition (CEEMD) [40] or the Ensemble Empirical Mode Decomposition (EEMD) [41].

The explained procedure has been applied to detect broken bars in directly-fed IM through the stator startup current, comparing its performance with the DWT [26]. The HHT presents some advantages in comparison to the DWT. For example, there is no need to choose an adequate mother wavelet. However, fault detection based in the Hilbert-Huang Spectrum (HHS) seems to be no superior to DWT. In [42], this last EMD implementation is used with vibration signals to extract fault patterns for bearing fault diagnosis.

Concerning inverter-fed IM, two interesting works [43], [44] utilize the HHT for diagnosis purposes, analyzing the stator current during the startup. The computing of the instantaneous energy of the HT of some specific IMF serves as fault severity quantification. The feasibility of the procedure is evaluated considering different IM operating conditions and voltage supplies.

The two signals proposed in this paper have been analyzed with this technique too. Both signals are decomposed into IMF with the EMD version proposed in [40] and with the following parameters: noise standard deviation: 0.1; 100 stages; 200 iterations and same noise level at all stages. In the case of the motor with one broken rotor bar, the EMD decomposes it into 16 IMF, but it fails in separating the oscillation modes corresponding to the LSH and USH from the mode corresponding to the FC. Their frequencies and mode oscillations are too close, and the EMD algorithm is not able to separate them. The signal of the motor with mixed eccentricity is decomposed into 12 IMF. The IMF number 4 contains the oscillation mode corresponding to the ERHn, but the ERHp is not separated from the FC. The IMF 4 and its HHS, showing the ERHn, are represented in Figs. 10(a) and (b) respectively.

F. ADAPTIVE SLOPE TRANSFORM

The Adaptive Slope Transform (AST) [23] belongs to the family of linear transforms, as the STFT or CWT. As explained before, linear transforms deliver a result with a tradeoff between time and frequency resolutions and this means that the evolution, instead of being represented by a perfectly thin line, it has a certain thickness. While the STFT has a constant tradeoff along the plane, and the CWT changes its tradeoff along frequency in a certain way imposed by its definition (being suitable only for capturing parabolic evolutions), the AST enables to fix a different tradeoff for each point of the t-f plane, optimizing the result everywhere. In other words, the tradeoff is adapted along the harmonic trajectories to minimize the thickness of the evolution being captured. As a consequence, the evolutions appear represented as thin as possible with this type of transform, and they can be better distinguished and characterized.

This approach has been applied to detect bar breakages in directly-fed IM [23]. Thanks to the transform adaptability, the BRB harmonics evolutions are completely captured during a complex transient, as a startup followed by load oscillations, even in regions where they evolve very close to the FC. This transform has also been applied to detect mixed eccentricity in inverter-fed IM [10].

The same approach used in [10] is employed to analyze the two currents of this paper (Figs. 11(a) and (c)). In the case of the motor with a bar breakage (Signal 1, Fig. 11 (a)), the slope criterion is applied to the FC evolution during the startup: its thickness is minimized. The trajectories of the BRB harmonics are almost parallel to the FC evolution (as analyzed in Fig. 1(b)). Therefore, according to the slope criterion, the atoms necessary in the t-f points along these evolutions are the same than those used along the FC trajectory. As explained in subsection B, the atom characteristics only depend on the time derivative of the frequency and in this case, the FC and the two BRB harmonics have the same. As a consequence, the atoms used during the startup (up to 11 s approximately), are the same in every point of the plane analyzed (Fig. 11 (b)). Nevertheless, the BRB harmonics are too close to the FC, and even with an FC minimum thickness, they fall inside the line representing the FC evolution, and cannot be detected (Fig. 11(a)), as with the STFT.

When the motor reaches the steady state (around 11 s in Fig. 11(a)), the frequency resolution is increased thanks to the AST adaptability, so the FC thickness along the frequency axis decreases. It can be seen how, after 11 s, the atom's characteristics start to change (Fig. 11(b)), being longer in time and shorter in frequency, to achieve that increase in the frequency resolution. Since the FC and the BRB harmonics evolutions are still parallel, the needed tradeoff between t-f resolutions continues to be the same for the three trajectories. Therefore, the atom's characteristics only change in time, being the same for every frequency related to a given instant. Since the frequency resolution increases, the BRB harmonics can be better separated and distinguished from the FC than in the STFT case (Fig. 7(a)).

In the case of the motor with mixed eccentricity (Signal 2, Fig. 11(c)), the slope criterion is also applied to optimize the FC capture during the startup. The AST enables to apply a different tradeoff along the mixed eccentricity harmonics evolutions during the startup. Nevertheless, the slopes of these trajectories are not different enough from that of the FC. Therefore, there would not be a big difference, and the same tradeoff is applied along the mixed eccentricity evolutions as with the FC. As a consequence, the atoms used during the startup (up to 2.2 s approximately), are the same for every point of the plane analyzed (Fig. 11(d)).

The tradeoff changes when the steady state is reached (around 2.2 s in Fig. 11(c)), as with Signal 1. More precisely, the frequency resolution increases, and we can observe how the thickness along the frequency axis of the lines representing the evolutions of the harmonics decreases, until appearing as thinner lines beyond the third second. This enables a better observation of the harmonics during the steady state, being able to separate and distinguish their frequencies better and to achieve this, the atoms start being longer in time and shorter in frequency (Fig. 11(d)), similarly to the family of atoms used with Signal 1. Therefore, with the AST, the shape of the atom can be adapted dynamically to the slope of the trajectories of the fault harmonics in the t-f plane, and the result is a good resolution both in the transient regime and in steady state.

Concluding, the AST applied in inverter-fed IM changes the tradeoff along time to optimize the capture of the FC, not only during startup but also during the steady state, and uses this same tradeoff along the fault harmonics evolutions, since their slopes are similar enough. This results in a good resolution during the startup and the stationary regime as well. In directly-fed IM [23], the adaptability of the transform

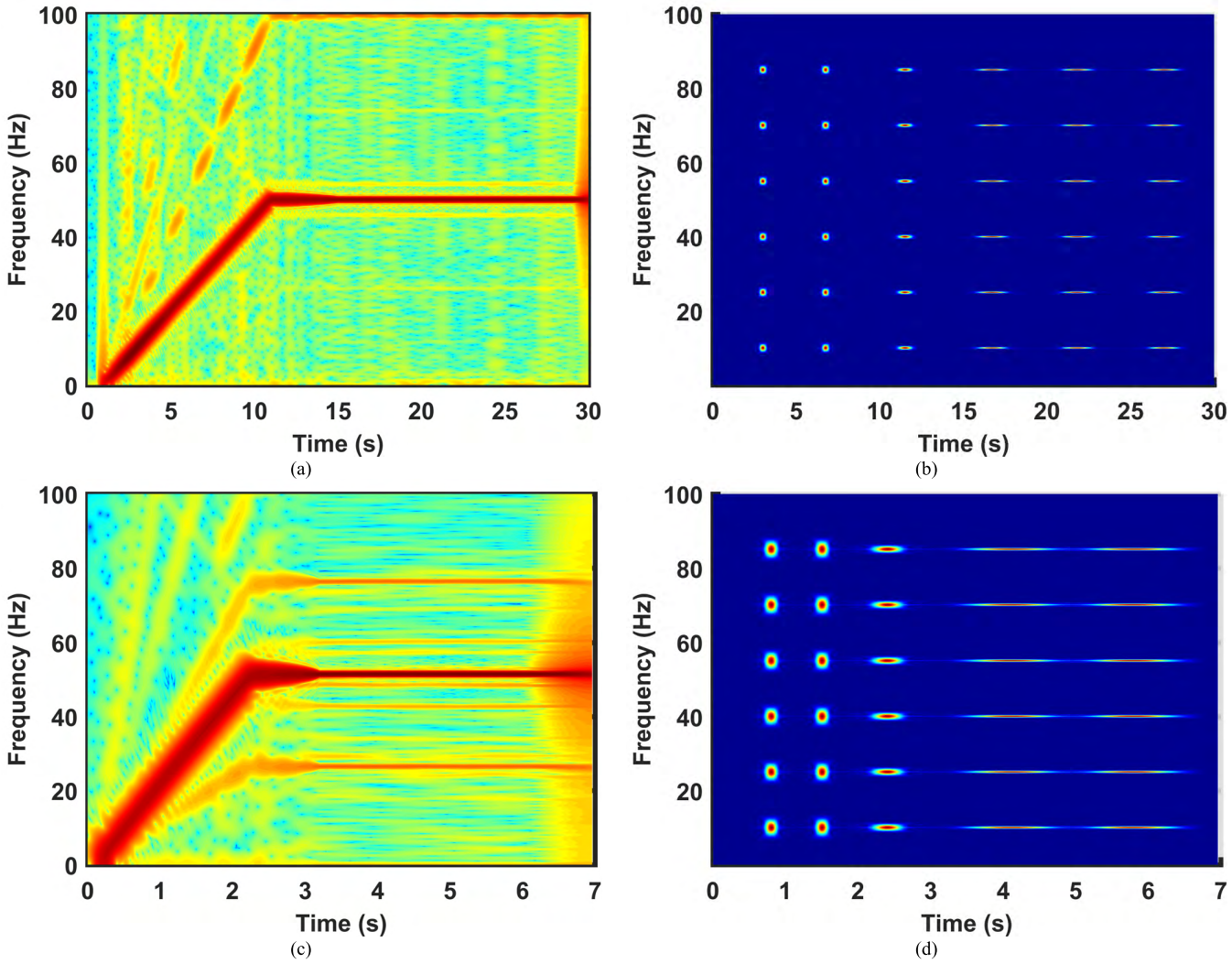

FIGURE 11. AST spectrograms and atoms for Signal 1 ((a) and (b)) and for Signal 2 ((c) and (d)).

makes a higher difference, since the evolutions of the FC and the faulty harmonics are completely different.

G. CHIRPLET TRANSFORM

The Chirplet Transform (CT) is a linear transform as the STFT, CWT, and AST. Nevertheless, this transform does not have a tradeoff between time and frequency resolutions when capturing an evolution following a straight line. In other words, the previous linear transforms represent the trajectory of a harmonic with a certain thickness. This thickness is the dispersion of the component's energy around its real evolution (caused by the transform used), which can be measured along the time and frequency axes. If the atom used is long in time, this thickness will be big along the time axis. If the atom used is long in frequency, this thickness will be significant along the frequency axis. In the case of the CT, the dispersion of the component's energy appears along the evolution of the component itself when it follows a straight line, achieving to represent it with a much lower thickness. This is achieved by using t-f atoms whose energy is distributed from its center mainly along a certain direction (Figs. 13(b) and (d)).

The main problem of the CT is that the user has to choose along which direction of the t-f plane the energy disperses. The CT can be applied to optimize the capture of one harmonic with a straight-line evolution, choosing its direction to disperse the energy of the atom. If the trajectory of the component changes from the straight line at some point of the transient captured, beyond that point, the capture would not be optimal. Moreover, if other harmonics are evolving in straight lines, but with different slopes, their capture would not be optimal either. This is caused by the fact that once the direction along which the atom's energy disperses is chosen, this direction is the same for every atom used, no matter at which point of the t-f plane is centered.

This technique has been used with success to detect for the first time broken bars during the startup of an inverter-fed IM [3]. This same approach has been used to analyze the two currents in the present paper. The CT has been applied

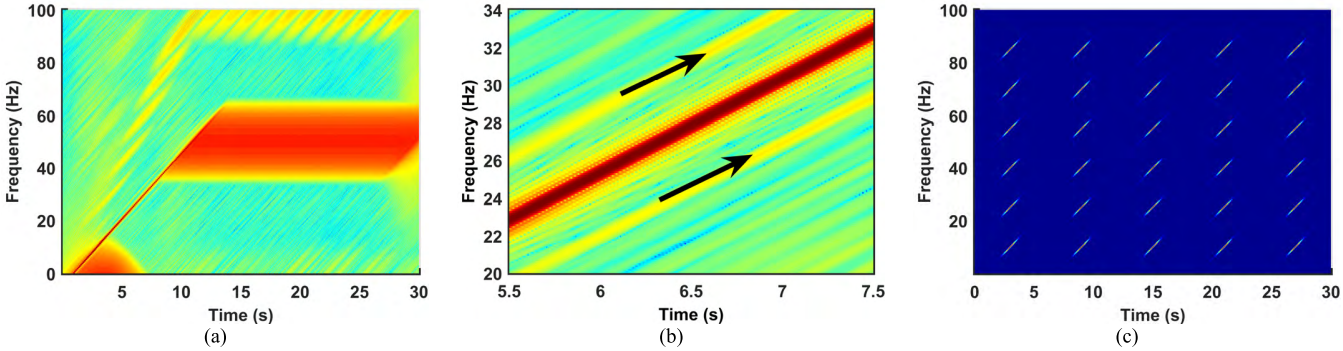

FIGURE 12. Result of the application of Chirplet Transform to Signal 1: (a) complete result; (b) detail with the BRB harmonics marked with black arrows; (c) family of atoms.

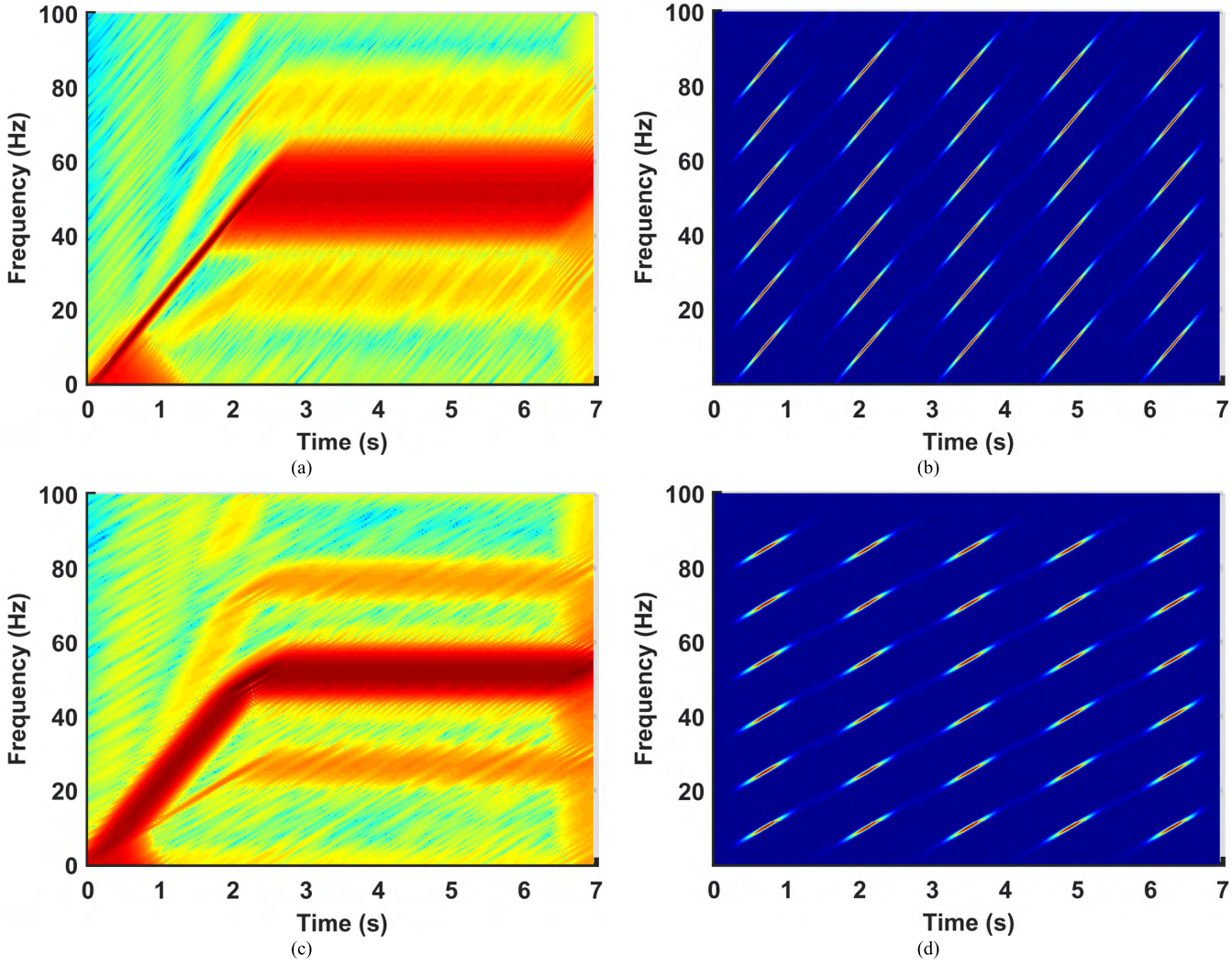

FIGURE 13. Result of the application of Chirplet Transform; spectrograms and atoms for Signal 1 ((a) and (b)) and for Signal 2 ((c) and (d)).

to Signal 1 to optimize the capture of the FC during the startup. As a consequence, its evolution during the startup appears (Fig. 12(a)) as a very thin line. The trajectories of the BRB harmonics are almost parallel to the FC in inverter-fed IM (as seen in Fig. 1(b)). Therefore, the CT analysis, which optimizes the capture of the FC during the startup, also optimizes the capture of the BRB harmonics during the startup. Fig. 12(c) shows the family of atoms that have been used: their energies dispersing along the same direction in which the FC and the BRB harmonics evolve during the

startup. As a result, the resolution during the transient regime is optimal to follow the evolution of the LSH and USH (see zoom, Fig. 12(b) where the BRB harmonics are marked with black arrows). The time and frequency resolution achieved permits a precise observation of the LSH and USH evolutions during the whole startup (even if they are close to the FC, as in this case). Nevertheless, the results during the final steady state are much worse than with previous transforms. Here, the energy of the FC is spread along its direction during the startup, highly increasing its thickness during steady state, and covering the trajectories of the LSH and USH.

Fig. 13 demonstrates the application of the CT to the motor with mixed eccentricity (Signal 2). The CT has been applied twice to Signal 2. First, the FC evolution has been optimally captured during the startup. For that purpose, atoms whose energy disperse along the direction of the FC evolution during the startup have been used (Fig. 13 (b)). The trajectory of the faulty harmonics (ERHp and ERHn) is now not so favorable because their respective slopes are different from the one of the FC. The fault related harmonics are observable during the startup from an earlier instant with respect to previous results, since the FC energy disperses less. Nevertheless, these evolutions appear blurred, especially during the steady state, where the type of analysis seems to be completely inadequate. In the steady state, the energy of the FC and the mixed-eccentricity harmonics spread over a wide area along the direction of the FC during the startup.

In the second analysis (Fig. 13 (c)), the energy of the atoms used disperses along the direction of the ERHn during the startup (Fig. 13(d)). As a result, the evolution of that fault harmonic is better captured during the startup, being represented by a thin line. Nevertheless, the thickness of the FC evolution during the startup increases, together with that of the ERHp. Since the slope of the direction along which the atom's energy disperses in this second analysis is smaller than for the first one (comparing Figs. 13(b) and (d)), the thickness of the evolutions during the steady state is smaller. The atoms are more similar to the horizontal atom that are necessary for this final steady state.

V. CONCLUSIONS

The detection of faulty components in the stator current of inverter-fed IM is a challenging problem, due to the proximity of their evolutions with the FC, and the continuous change of the FC frequency during transients. The comparison of the main t-f techniques to solve this problem (presented in this paper) is summarized below, as a guide for the field engineers, and for researchers who want to know how far each technique has reached, which the most hopeful paths are, and what results should still be sought.

The STFT has a fixed t-f resolution tradeoff along the plane, which is sufficient to obtain the evolution of the mixed eccentricity components, but it fails when diagnosing bar breakages during the startup.

The CWT enables a variable tradeoff with the frequency analyzed. Nevertheless, the way it varies is not suited for the types of evolutions of the components in induction motor stator currents, and it should be avoided.

The DWT decomposes the current into subsignals related to different frequency bands, but it does not allow to obtain the evolutions since the presence of the FC in all the subsignals obtained masks the faulty components.

The WVD eliminates the t-f resolution tradeoff, but it introduces cross-terms. Since the FC and its harmonics cannot be filtered as in the directly-fed case, the cross-terms effects are not decreased, and only some traces of the mixed eccentricity harmonics are observed.

The HHT tries to split the current into its components, and then to obtain their instantaneous frequency. Nevertheless, it only succeeds to separate the lower mixed eccentricity component from the stator current.

The AST offers a completely adaptable t-f resolution tradeoff which improves the STFT performance. Nevertheless, the bar breakage components are not yet detected during the startup.

The CT eliminates the t-f resolution tradeoff of the previous transforms without introducing cross-terms. As a consequence, the bar breakage components are finally captured during the startup. Nevertheless, the mixed eccentricity result does not improve with respect to the AST.

Concluding, the STFT is a good option to detect mixed eccentricity, while the AST must be used to obtain optimized results. Only the CT is suitable to detect bar breakages.

REFERENCES

[1] J. Tolvanen, "Saving energy with variable speed drives," *World Pumps*, vol. 2008, no. 501, pp. 32–33, Jun. 2008.

[2] C. M. F. S. Reza, M. D. Islam, and S. Mekhilef, "A review of reliable and energy efficient direct torque controlled induction motor drives," *Renew. Sustain. Energy Rev.*, vol. 37, pp. 919–932, Sep. 2014.

[3] J. Pons-Llinares, D. Morinigo-Sotelo, O. Duque-Perez, J. Antonino-Daviu, and M. Perez-Alonso, "Transient detection of close components through the chirplet transform: Rotor faults in inverter-fed induction motors," in *Proc. 40th Annu. Conf. IEEE Ind. Electron. Soc. (IECON)*, Oct./Nov. 2014, pp. 3386–3392.

[4] R. Saidur, S. Mekhilef, M. B. Ali, A. Safari, and H. A. Mohammed, "Applications of variable speed drive (VSD) in electrical motors energy savings," *Renew. Sustain. Energy Rev.*, vol. 16, no. 1, pp. 543–550, Jan. 2012.

[5] V. Ghorbanian and J. Faiz, "A survey on time and frequency characteristics of induction motors with broken rotor bars in line-start and inverter-fed modes," *Mech. Syst. Signal Process.*, vols. 54–55, pp. 427–456, Mar. 2015.

[6] H. Henao, H. Razik, and G.-A. Capolino, "Analytical approach of the stator current frequency harmonics computation for detection of induction machine rotor faults," *IEEE Trans. Ind. Appl.*, vol. 41, no. 3, pp. 801–807, May/Jun. 2005.

[7] J.-H. Jung, J.-J. Lee, and B.-H. Kwon, "Online diagnosis of induction motors using MCSA," *IEEE Trans. Ind. Electron.*, vol. 53, no. 6, pp. 1842–1852, Dec. 2006.

[8] J. P. Amezquita-Sanchez, M. Valtierra-Rodriguez, D. Camarena-Martinez, D. Granados-Lieberman, R. J. Romero-Troncoso, and A. Dominguez-Gonzalez, "Fractal dimension-based approach for detection of multiple combined faults on induction motors," *J. Vibrat. Control*, vol. 22, no. 17, pp. 3638–3648, Jan. 2015.

[9] V. Climente-Alarcon, J. A. Antonino-Daviu, F. Vedreno-Santos, and R. Puche-Panadero, "Vibration transient detection of broken rotor bars by PSH sidebands," *IEEE Trans. Ind. Appl.*, vol. 49, no. 6, pp. 2576–2582, Nov./Dec. 2013.

[10] J. Pons-Llinares, J. Antonino-Daviu, J. Roger-Folch, D. Morinigo-Sotelo, and O. Duque-Pérez, "Mixed eccentricity diagnosis in inverter-fed induction motors via the adaptive slope transform of transient stator currents," *Mech. Syst. Signal Process.*, vol. 48, pp. 423–435, Oct. 2014.
[11] D. Morinigo-Sotelo, L. A. Garcia-Escudero, O. Duque-Perez, and M. Perez-Alonso, "Practical aspects of mixed-eccentricity detection in PWM voltage-source-inverter-fed induction motors," *IEEE Trans. Ind. Electron.*, vol. 57, no. 1, pp. 252–262, Jan. 2010.
[12] W. S. Abu-Elhaija, V. Ghorbanian, J. Faiz, and B. M. Ebrahimi, "Impact of closed-loop control on behavior of inverter-fed induction motors with rotor broken-bars fault," in *Proc. IEEE Int. Conf. Power Electron., Drives Energy Syst. (PEDES)*, Dec. 2012, pp. 1–4.
[13] J. Faiz, V. Ghorbanian, and B. M. Ebrahimi, "A survey on condition monitoring and fault diagnosis in line-start and inverter-fed broken bar induction motors," in *Proc. IEEE Int. Conf. Power Electron., Drives Energy Syst. (PEDES)*, Dec. 2012, pp. 1–5.
[14] M. Riera-Guasp *et al.*, "Diagnosis of induction machines under non-stationary conditions: Concepts and tools," in *Proc. IEEE Workshop Elect. Mach. Design Control Diagnosis (WEMDCD)*, Mar. 2013, pp. 220–231.
[15] J. Pons-Llinares, V. Climente-Alarcon, F. Vedreno-Santos, J. Antonino-Daviu, and M. Riera-Guasp, "Electric machines diagnosis techniques via transient current analysis," in *Proc. 38th Annu. Conf. IEEE Ind. Electron.*, Oct. 2012, pp. 3893–3900.
[16] V. Fernandez-Cavero, D. Morinigo-Sotelo, O. Duque-Perez, and J. Pons-Llinares, "Fault detection in inverter-fed induction motors in transient regime: State of the art," in *Proc. IEEE 10th Int. Symp. Diagnostics Elect. Mach., Power Electron. Drives (SDEMPED)*, Sep. 2015, pp. 205–211.
[17] W. Deleroi, "Broken bar in a squirrel-cage rotor of an induction motor—Description by superimposed fault-currents," *Arch. Elektrotechnik*, vol. 67, no. 2, pp. 91–99, 1984.
[18] J. R. Cameron, W. T. Thomson, and A. B. Dow, "Vibration and current monitoring for detecting airgap eccentricity in large induction motors," *IEE Proc. B-Electr. Power Appl.*, vol. 133, no. 3, pp. 155–163, May 1986.
[19] M. Riera-Guasp, J. A. Antonino-Daviu, M. Pineda-Sanchez, R. Puche-Panadero, and J. Perez-Cruz, "A general approach for the transient detection of slip-dependent fault components based on the discrete wavelet transform," *IEEE Trans. Ind. Electron.*, vol. 55, no. 12, pp. 4167–4180, Dec. 2008.
[20] V. T. Tran, F. AlThobiani, A. Ball, and B.-K. Choi, "An application to transient current signal based induction motor fault diagnosis of Fourier–Bessel expansion and simplified fuzzy ARTMAP," *Expert Syst. Appl.*, vol. 40, no. 13, pp. 5372–5384, 2013.
[21] M. Pineda-Sanchez, M. Riera-Guasp, J. A. Antonino-Daviu, J. Roger-Folch, J. Perez-Cruz, and R. Puche-Panadero, "Diagnosis of induction motor faults in the fractional Fourier domain," *IEEE Trans. Instrum. Meas.*, vol. 59, no. 8, pp. 2065–2075, Aug. 2010.
[22] B. Yazici and G. B. Kliman, "An adaptive statistical time-frequency method for detection of broken bars and bearing faults in motors using stator current," *IEEE Trans. Ind. Appl.*, vol. 35, no. 2, pp. 442–452, Mar. 1999.
[23] J. Pons-Llinares, M. Riera-Guasp, J. A. Antonino-Daviu, and T. G. Habetler, "Pursuing optimal electric machines transient diagnosis: The adaptive slope transform," *Mech. Syst. Signal Process.*, vol. 80, pp. 553–569, Dec. 2016.
[24] J. Cusidó, L. Romeral, J. A. Ortega, J. A. Rosero, and A. G. Espinosa, "Fault detection in induction machines using power spectral density in wavelet decomposition," *IEEE Trans. Ind. Electron.*, vol. 55, no. 2, pp. 633–643, Feb. 2008.
[25] S. Mallat, *A Wavelet Tour of Signal Processing*, 3rd ed. Burlington, MA, USA: Academic, 2009.
[26] J. A. Antonino-Daviu, M. Riera-Guasp, M. Pineda-Sanchez, and R. B. Pérez, "A critical comparison between DWT and Hilbert–Huang-based methods for the diagnosis of rotor bar failures in induction machines," *IEEE Trans. Ind. Appl.*, vol. 45, no. 5, pp. 1794–1804, Sep./Oct. 2009.
[27] J. Pons-Llinares, J. A. Antonino-Daviu, M. Riera-Guasp, M. Pineda Sanchez, and V. Climente-Alarcon, "Induction motor diagnosis based on a transient current analytic wavelet transform via frequency B-splines," *IEEE Trans. Ind. Electron.*, vol. 58, no. 5, pp. 1530–1554, May 2011.
[28] M. Pineda-Sanchez, M. Riera-Guasp, J. Perez-Cruz, and R. Puche-Panadero, "Transient motor current signature analysis via modulus of the continuous complex wavelet: A pattern approach," *Energy Convers. Manage.*, vol. 73, pp. 26–36, Sep. 2013.
[29] J. Pons-Llinares, J. Antonino-Daviu, J. Roger-Folch, D. Morinigo-Sotelo, and O. Duque-Perez, "Eccentricity diagnosis in inverter-fed induction motors via the analytic wavelet transform of transient currents," in *Proc. 19th Int. Conf. Elect. Mach. (ICEM)*, Sep. 2010, pp. 1–6.
[30] M. Riera-Guasp, J. A. Antonino-Daviu, J. Roger-Folch, and M. P. M. Palomares, "The use of the wavelet approximation signal as a tool for the diagnosis of rotor bar failures," *IEEE Trans. Ind. Appl.*, vol. 44, no. 3, pp. 716–726, May/Jun. 2008.
[31] K. Yahia, A. J. M. Cardoso, A. Ghoggal, and S.-E. Zouzou, "Induction motors broken rotor bars diagnosis through the discrete wavelet transform of the instantaneous reactive power signal under time-varying load conditions," *Electr. Power Compon. Syst.*, vol. 42, no. 7, pp. 682–692, 2014.
[32] K. Yahia, A. J. M. Cardoso, A. Ghoggal, and S. E. Zouzou, "Induction motors airgap-eccentricity detection through the discrete wavelet transform of the apparent power signal under non-stationary operating conditions," *ISA Trans.*, vol. 53, no. 2, pp. 603–611, Mar. 2014.
[33] K. Teotrakool, M. J. Devaney, and L. Eren, "Adjustable-speed drive bearing-fault detection via wavelet packet decomposition," *IEEE Trans. Instrum. Meas.*, vol. 58, no. 8, pp. 2747–2754, Aug. 2009.
[34] M. Dlamini, P. S. Barendse, and A. M. Khan, "Detecting faults in inverter-fed induction motors during startup transient conditions," in *Proc. IEEE Energy Convers. Congr. Expo.*, Sep. 2014, pp. 3131–3138.
[35] F. Hlawatsch and F. Auger, Eds., *Time-Frequency Analysis: Concepts and Methods*. London, U.K.: ISTE, 2008.
[36] V. Climente-Alarcon, J. A. Antonino-Daviu, M. Riera-Guasp, R. Puche-Panadero, and L. Escobar, "Application of the Wigner–Ville distribution for the detection of rotor asymmetries and eccentricity through high-order harmonics," *Electr. Power Syst. Res.*, vol. 91, pp. 28–36, Oct. 2012.
[37] V. Climente-Alarcon *et al.*, "Transient tracking of low and high-order eccentricity-related components in induction motors via TFD tools," *Mech. Syst. Signal Process.*, vol. 25, no. 2, pp. 667–679, Feb. 2011.
[38] V. Climente-Alarcon, J. A. Antonino-Daviu, A. Haavisto, and A. Arkkio, "Particle filter-based estimation of instantaneous frequency for the diagnosis of electrical asymmetries in induction machines," *IEEE Trans. Instrum. Meas.*, vol. 63, no. 10, pp. 2454–2463, Oct. 2014.
[39] M. Rajagopalan, J. A. Restrepo, J. M. Aller, T. G. Habetler, and R. G. Harley, "Nonstationary motor fault detection using recent quadratic time–frequency representations," *IEEE Trans. Ind. Appl.*, vol. 44, no. 3, pp. 735–744, May/Jun. 2008.
[40] M. E. Torres, M. A. Colominas, G. Schlotthauer, and P. Flandrin, "A complete ensemble empirical mode decomposition with adaptive noise," in *Proc. IEEE Int. Conf. Acoust., Speech Signal Process.*, May 2011, pp. 4144–4147.
[41] Z. Wu and N. E. Huang, "Ensemble empirical mode decomposition: A noise-assisted data analysis method," *Adv. Adapt. Data Anal.*, vol. 1, no. 1, pp. 1–41, 2009.
[42] L. Meng, J. Xiang, Y. Wang, Y. Jiang, and H. Gao, "A hybrid fault diagnosis method using morphological filter–translation invariant wavelet and improved ensemble empirical mode decomposition," *Mech. Syst. Signal Process.*, vols. 50–51, pp. 101–115, Jan. 2015.
[43] J. Faiz, V. Ghorbanian, and B. M. Ebrahimi, "EMD-based analysis of industrial induction motors with broken rotor bars for identification of operating point at different supply modes," *IEEE Trans. Ind. Informat.*, vol. 10, no. 2, pp. 957–966, May 2014.
[44] J. Faiz, V. Ghorbanian, and B. M. Ebrahimi, "A new criterion for rotor broken bar fault diagnosis in line-start and inverter-fed induction motors using Hilbert–Huang transform," in *Proc. IEEE Int. Conf. Power Electron., Drives Energy Syst. (PEDES)*, Dec. 2012, pp. 1–6.

VANESSA FERNANDEZ-CAVERO received the B.S. degree in industrial organization engineering and electrical engineering from ICAI, Comillas Pontifical University, Madrid, Spain, in 2005. She is currently pursuing the Ph.D. degree with the University of Valladolid, Spain. Her current research interests include the monitoring of induction machines and the detection and diagnosis of faults in inverter-fed IM in transient regimes.

DANIEL MORINIGO-SOTELO (M'04) received the B.S. and Ph.D. degrees in electrical engineering from the University of Valladolid (UVA), Spain, in 1999 and 2006, respectively. He was a Research Collaborator on Electromagnetic Processing of Materials with the Light Alloys Division of CIDAUT Foundation since 2000 until 2015. He is currently with the Research Group in Predictive Maintenance and Testing of Electrical Machines, Department of Electrical Engineering, UVA, and with the HSPdigital Research Group, Mexico. His current research interests include the condition monitoring of induction machines, optimal electromagnetic design, and heuristic optimization.

OSCAR DUQUE-PEREZ received the B.S. and Ph.D. degrees in electrical engineering from the University of Valladolid (UVA), Spain, in 1992 and 2000, respectively. In 1994, he joined the E.T.S. de Ingenieros Industriales, UVA, where he is currently a Full Professor with the Research Group in Predictive Maintenance and Testing of Electrical Machines, Department of Electrical Engineering. His main research interests include power systems reliability, condition monitoring, and heuristic optimization techniques.

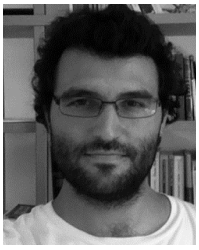

JOAN PONS-LLINARES (M'13) received the M.Sc. degree in industrial engineering and the Ph.D. degree in electrical engineering from the Universitat Politècnica de València (UPV), Valencia, Spain, in 2007 and 2013, respectively. He is currently an Assistant Professor with the Department of Electrical Engineering, UPV. His research interests include time-frequency transforms, condition monitoring, and the diagnostics of electrical machines.